SCIENTIFIC CULTURE
www.sci-cult.com

SCIENTIFIC CULTURE, Vol. 9, No. 3, (2023), pp. 73-87
Open Access. Online & Print

DOI: 10.5281/zenodo.7978086

DIGITAL MODELLING OF CERAMIC SHERDS BY MEANS OF PHOTOGRAMMETRY AND MACROPHOTOGRAPHY: UNCERTAINTY CALCULATIONS AND MEASUREMENT ERRORS

Michail I. Stamatopoulos and Christos-Nikolaos Anagnostopoulos*

Intelligent Systems lab (i-lab),
Cultural Technology and Communication Dpt., Social Sciences School,
University of the Aegean, Lesvos isl., Mytilene, 81100, Greece

Received: 12/07/2023
Accepted: 01/08/2023
Corresponding author: Christos-Nikolaos Anagnostopoulos (canag@aegean.gr)

ABSTRACT

Photogrammetry has emerged as a valuable technique for digitizing real-world objects. In the field of archaeology, the generation of realistic 3D models from 2D images has become a preferred method for scholars engaged in excavation, conservation, and restoration work. While the concept of modelling entire excavations or small objects from various angles is exciting, the precision and realism of 3D models remain areas of investigation. Initially, photogrammetric techniques were primarily used for large-scale or medium-scale objects. However, in recent years, there has been a growing interest in applying photogrammetry to model small-scale objects. The crucial question for small objects, ranging from a few centimeters to a few tens of centimeters in size, is whether photogrammetry can produce high-precision 3D models. This paper focuses on a small ceramic sherd from a handmade replica of a large red-figure amphora. Through an iterative process involving photogrammetry and macrophotography (close-up photography), ten different digital models of the sherd are generated. From each of these models, thickness measurements are extracted at 24 specific points, allowing for a comparison and calculation of uncertainties associated with these measurements. The dispersion of the measurements around the mean value provides an estimation of the actual size values and measurement errors, enabling an evaluation of the precision of photogrammetry in size recognition. Furthermore, the same sherd is measured ten times using a caliper at the same points, and the thickness measurements are compared to calculate the uncertainties of the caliper measurements. By estimating the sizes and their respective errors, the measurement error of the photogrammetry technique can be determined. Overall, this study aims to investigate the precision of photogrammetry in generating high-precision 3D models and compare it to the measurements obtained from a caliper.

KEYWORDS: Thickness Profile, Sherds, Pottery Reassembly, Virtual Reconstruction, Digital Reassembling

1. INTRODUCTION

Ἐπειδὴ τὸ εἰδέναι καὶ τὸ ἐπίστασθαι συμβαίνει περὶ πάσας τὰς μεθόδους, ὧν εἰσὶν ἀρχαὶ ἢ αἴτια ἢ στοιχεῖα, ἐκ τοῦ ταῦτα γνωρίζειν, δῆλον ὅτι καὶ τῆς περὶ φύσεως ἐπιστήμης πειρατέον διορίσασθαι πρῶτον τὰ περὶ τὰς ἀρχάς. ARISTOTLE'S, PHYSICS, Book I, 184a.10, 184a.11, 184a.12, 184a.14, 184a.15, 184a.16.

(Translation: Since, knowing and being knowing with certainty, of something that occurs within the range of action of methods which possess principles, reasons and fundamental elements, through which one can say that he is really aware of some-thing, it is obvious and evident that in the case of natural sciences too, our priority should be to attempt clearly determine everything around their principles).

The outcome obtained from observing and counting a natural quantity typically includes an indeterminate percentage of error, referred to as uncertainty or randomness. The disparity between each measurement and its true value, which remains unknown, is known as measurement error. This uncertainty, along with the resulting errors, can arise from various random factors (such as temperature, pressure, lighting, interference) as well as systematic factors (like instrument imperfections, incorrect calibrations). These factors are widely recognized, underscoring the importance of determining and quantifying the reliability of the results produced by each measurement process (Bevington and Robinson, 2003; BIPM et al., 1995; BIPM et al., 2020).

This paper focuses on the calculation and determination of measurement errors in three-dimensional (3D) digital models of small ceramic fragments (sherds or *ostraca*) created using cutting-edge technologies, which are the technique of generation, realistic 3D digital models from 2D images (photogrammetry) and the technique of taking close-up photographs on small subjects (macrophotography). Sherds, which are small objects characterized by complex geometry and significant differences in height, length, and width, are particularly suitable for digital 3D modelling using photogrammetry and macrophotography (see Fig. 1). By selecting sample measurements from a collection of digital models of a small sherd, it becomes possible to draw reliable conclusions about the overall uncertainty, which can be extrapolated to the broader population of similar measurements.

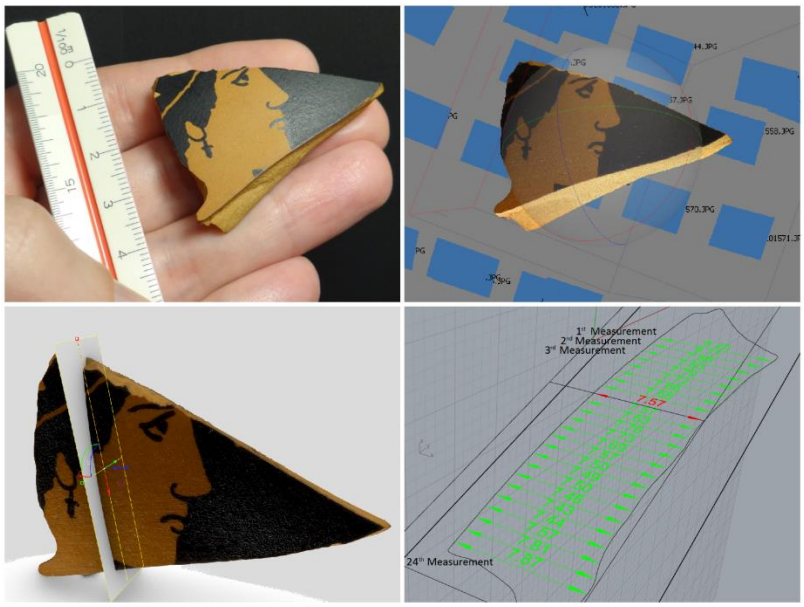

Figure 1. The small ceramic sherd (4.8 x 3.5 x 0.8 cm). The real object, the digital model and the extracted measurements.

2. PHOTOGRAMMETRY AND MACRO-PHOTOGRAPHY

2.1. Photogrammetry

Photogrammetry, a technique used to generate three-dimensional (3D) digital models, has proven successful in modelling objects of large or medium scale. By capturing photographs of such objects from multiple viewpoints and angles using a simple camera, they can be easily converted into 3D digital representations (Luhmann, 2010; Peggs et al., 2009). However, the applicability of this method extends beyond larger objects and should not be limited to them (Mendikute et al., 2017; Percoco et al., 2017). The emergence of nanotechnology in materials research has created a growing demand for digital modelling of micro-scale and even nano-scale objects (Mallison and Wings, 2014; Vaezi et al., 2013). Photogrammetry

holds the potential to faithfully and realistically recreate highly precise models of many small complex objects, ranging from a few centimeters to just a few millimeters in size (Gontard et al., 2018; Remondino et al., 2012; Yanagi and Chikatsu, 2010).

In the field of archaeology, small ceramic fragments known as sherds, coins found in archaeological museums, materials retrieved from ancient shipwrecks, or artifacts from Paleolithic excavations are examples of precious objects that demand precision at the millimeter-level or even finer measurements (Samaan et al., 2013; Puhar et al., 2018; Marziali and Dionisio, 2017). As discussed earlier, photogrammetry, a method commonly used for modelling objects of medium size, presents a relatively affordable option and is readily embraced by new researchers. However, utilizing photogrammetry effectively requires expertise, as it is a delicate process sensitive to factors like lighting variations, shadows, vibrations, reflections, and other considerations.

2.2. *Photogrammetry and Macrophotography*

Small objects with intricate shapes, where there is a significant disparity between the object's height and its length or width, present unique challenges when it comes to digital modelling using photogrammetry. In such cases, a conventional photographic lens is inadequate as it cannot easily capture close-up details, resulting in less accurate models. Likewise, optical scanners such as laser scanners or 3D scanners face a similar limitation due to their size, making it difficult to approach small subjects from very close distances. However, advancements in digital photography and the enhanced imaging capabilities have enabled photogrammetry to overcome this obstacle with the assistance of macrophotography (Santella and Milner, 2017). Macrophotography, is the technique of taking close-up photographs of small subjects (butterflies, flowers, coins, etc.), for revealing details, often-overlooked details in everyday life. Specialized macrophotographic lenses can get extremely close to an object, down to millimeter-level precision, and capture even the smallest details. Macrophotography vary from microphotography as, microphotography is a more specialized type of photography that involves capturing details of microscopic subjects (microorganisms, bacteria, etc.), that are not visible to the naked eye and requires specialized equipment, such microscopes. Nonetheless, these approaches introduce new challenges, including micro-vibrations, small focal depth, and the resulting limitation of focusing on a small area of the object (Kraus, 2007; Ray, 2002). The latter problem implies that each photo in the photography set has relatively few overlapping points with other photos, necessitating a larger number of photos to establish correlations between them using photogrammetry software. This, in turn, leads to a more complex photo set with numerous images, thereby significantly increasing the processing time required by the photogrammetry software. Developing the digital model of small objects using the combination of photogrammetry and macrophotography, particularly when a 360-degree photographic scan is required in both horizontal and vertical planes, poses even greater challenges due to the necessity of capturing a significantly larger number of photos. These challenges collectively contribute to the complexity of digital modelling for small objects using photogrammetry and macrophotography, an area that remains an active field of research (Gajski et al., 2016).

2.3. *Photogrammetry, Macrophotography and Precision at a reduced length scale*

The accuracy and realism of any 3D digital model created through photogrammetry naturally raise questions regarding acceptable levels of horizontal and vertical error. The answer to this question may vary depending on the specific field of application, such as archaeology, mechanical engineering, criminology, entomology, and so on. When modelling large-scale objects like an archaeologically significant building facade (Murtiyoso et al., 2017) or an excavation site (Cramer, 2013; Quattrini et al., 2017), an error of around 10 millimeters in the horizontal or vertical measurements may be considered acceptable. However, for small objects such as a bullet from a ballistic test or a capillary crack in an aircraft wing (Jing et al., 2015), a much higher level of measurement accuracy is required.

To validate the horizontal and vertical accuracy of scaled-down models, recent scientific studies have placed significant emphasis on addressing model deformation and introducing error estimates to assess the reliability of the obtained quantities (Plum and Labonte, 2021; Stamatopoulos and Fraser, 2011; Mikerov et al., 2020). Various techniques are employed for this purpose, including the use of specific target points (Stamatopoulos and Fraser, 2014; Xu and Dudek, 2011), calibrated error assessment charts (Verma and Bourke, 2019), and scale bars. These methodologies contribute to ensuring the precision and credibility of the 3D model's measurements.

In order to verify the horizontal and vertical accuracy of digital models with reduced dimensions and complex geometry, a research project was conducted by the Intelligent Systems Laboratory (i-lab) at the University of the Aegean.

As part of this project, a small ceramic sherd, measuring 4.8 x 3.5 x 0.8 cm (see Fig. 1, top left), was selected. This sherd was obtained from a hand-made replica of a large amphora, which was intentionally

fragmented in the laboratory. The real red-figure style masterpiece, 50 cm tall, is exhibited as part (Cat. No. 571) of the permanent museum collection in the provincial museum *Sigismondo Castromediano* in Lecce, Italy, and is attributed to the Apulian painter of the Berlin Dancing Girl. The main scene of the amphora, narrates a farewell between Achilles and Briseis. This high precision handmade replica was built, fully decorated in our laboratory and then intentionally destroyed, giving us 507 fragments, out of which 148 sherds were offered for digital restoration through the *Thickness Profile method* on an on-going project (see Fig. 2). The *Thickness Profile method*, which facilitates the digital reassembly of fragmented archaeological ceramic pottery, was developed in 2016 and has been thoroughly described in our previous works (Stamatopoulos and Anagnostopoulos, 2017; Stamatopoulos and Anagnostopoulos, 2018).

The selected sherd (the Briseis face) was subjected to a 10-iteration process involving photogrammetry and macrophotography to generate digital 3D models (see Fig. 3). Using the Rhino-Rhinoceros digital processing software developed by Robert McNeel & Associates (depicted in Fig. 4), 10 different photographic sets were used to create 10 distinct digital 3D models. From these models, precise measurements of thickness were extracted from identical points. The measurements were recorded with an accuracy of hundredths of a millimeter (0.00 mm accuracy). For each of 10 digital 3D models, a total of 24 thickness measurements were obtained (see Fig. 4), and their uncertainties and errors were calculated and compared using formulas (2.1) to (2.8), as shown in Table I. The resulting uncertainties and errors are presented in Table III. The 24 points obtained from the digital models represent a two-dimensional vertical cross-section. This cross-section (see Fig. 4), is significant because, in the field of archaeology and ceramic studies, the classification, restoration, and reassembly of fragmented pottery (sherds) heavily rely on the examination of cross-sections, also known as profiles. These techniques encompass both digital and manual approaches. Therefore, this study aims to compare the profiles of real sherds, which archaeologists would typically analyze using a high-precision caliper, with the digital models reconstructed through photogrammetry and macrophotography. Prior to the analysis, the vertical cross-section was appropriately aligned through a process that involved matching the horizontal lines left on the inner side of the sherd by the potter's fingers during the pottery's construction. This alignment step is an integral part of implementing the *Thickness Profile method*.

Based on the dispersion of thickness measurements around the mean value (standard deviation), the actual sizes of the ceramic sherd are estimated, along with the corresponding measurement errors at the 24 points in the 10 digital models. This estimation helps determine the accuracy with which photogrammetry and macrophotography recognize the sizes. Additionally, the same ceramic sherd is independently measured 10 times at the exact same points using a precision caliper. For these caliper measurements, 24 thickness values, as shown in Table II, are obtained with an accuracy of hundredths of a millimeter (0.00 mm accuracy). To assess the uncertainties and errors in these caliper measurements, formulas (2.1) to (2.8) described in Table I are utilized. The uncertainties and errors of these caliper measurements are presented in Table IV. The caliper used in the measurements is calibrated and checked for accuracy using a special ceramic gage block of high precision (grade 1).

Once all the magnitudes and their respective errors ($\alpha \pm \delta\alpha$) and ($\beta \pm \delta\beta$) have been calculated, the error in photogrammetry relative to the real-world data is emphasized.

It is assumed that the variation in all measurements, both from the digital models and the caliper, follows a normal probability distribution, specifically a Gaussian distribution (normal distribution), with a probability of approximately 68%.

Figure 2. The amphora, from the building up process to the breakage stage. On the left, the real object (Cat. No. 571) in the provincial museum Sigismondo Castromediano in Lecce, Italy.

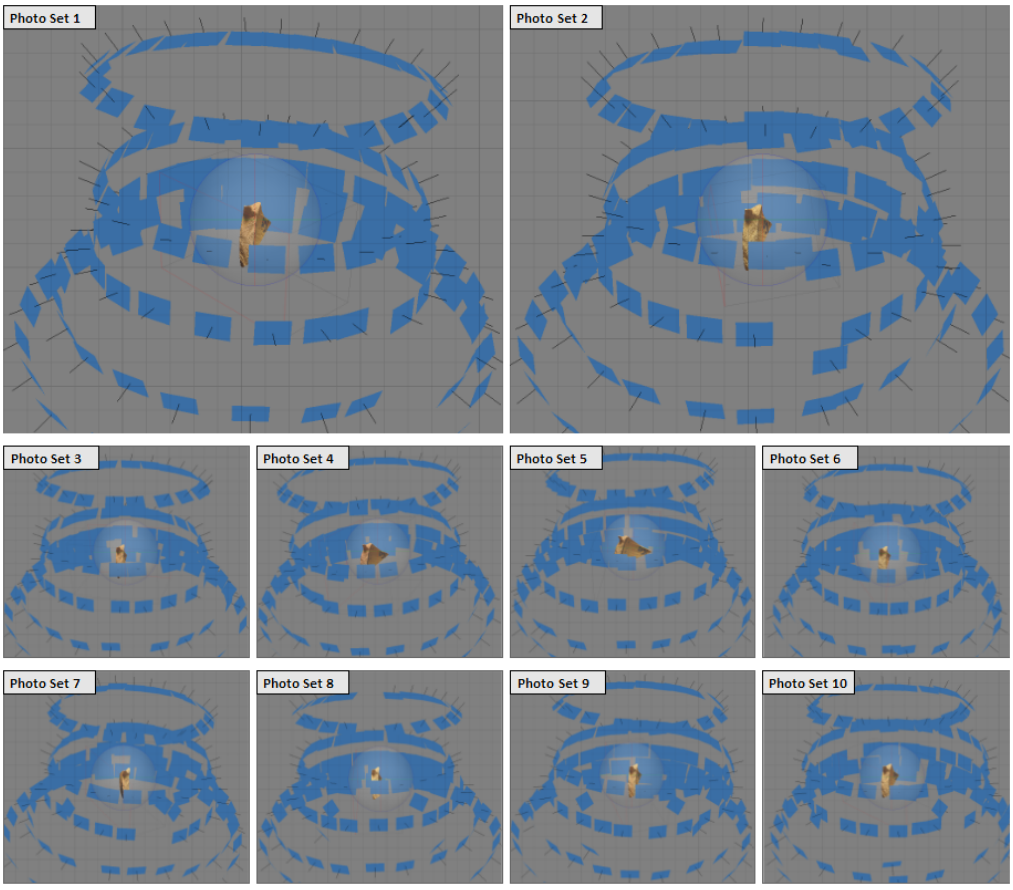

	Photo Set 1	Photo Set 2	Photo Set 3	Photo Set 4	Photo Set 5
Photographs	118	118	116	120	120
Targets	20	21	19	21	17
Point Cloud					
Points	33,381 of 83,989	38,058 of 88,286	31,227 of 78,701	33,387 of 84,803	33,301 of 84,128
RMS reprojection error	0.180827 (1.18106 pix)	0.180633 (1.14053 pix)	0.166336 (1.11974 pix)	0.175287 (1.17871 pix)	0.176446 (1.19543 pix)
Max reprojection error	0.557087 (28.8866 pix)	0.553965 (30.1705 pix)	0.515611 (29.2099 pix)	0.540558 (28.332 pix)	0.543427 (28.3337 pix)
Dense Point Cloud					
Points	5,128,914	4,667,597	4,661,738	5,543,887	5,421,945
Model					
Faces	83,150	142,536	125,488	79,862	68,724
Vertices	41,576	71,258	62,744	39,940	34,363

	Photo Set 6	Photo Set 7	Photo Set 8	Photo Set 9	Photo Set 10
Photographs	120	120	120	120	120
Targets	19	19	22	20	21
Point Cloud					
Points	35,766 of 84,745	33,899 of 85,407	37,753 of 90,235	37,137 of 89,409	33,225 of 84,511
RMS reprojection error	0.174282 (1.09333 pix)	0.174819 (1.21762 pix)	0.172321 (1.10788 pix)	0.176904 (1.13263 pix)	0.170231 (1.12541 pix)
Max reprojection error	0.536279 (29.639 pix)	0.536726 (26.3989 pix)	0.531203 (28.6609 pix)	0.542949 (23.76 pix)	0.524226 (28.0201 pix)
Dense Point Cloud					
Points	5,153,917	5,700,402	5,821,107	5,893,994	5,390,908
Model					
Faces	50,390	55,848	59,042	65,594	82,402
Vertices	25,195	27,927	29,523	32,794	41,200

airTemp (°C) mslPres (hPa) relHumi (%)		
Photo Set 1		
29.0	1010.9	20.
Photo Set 2		
28.6	1011.1	22.
Photo Set 3		
28.5	1011.0	20.
Photo Set 4		
28.7	1010.8	21.
Photo Set 5		
28.5	1010.9	22.
Photo Set 6		
29.0	1008.0	32.
Photo Set 7		
28.2	1006.8	47.
Photo Set 8		
29.0	1004.6	28.
Photo Set 9		
28.5	1005.5	53.
Photo Set 10		
28.0	1006.1	58.

Figure 3. The 10 different photo sets (120 shots per set) and the 10 digital 3D models from the same small ceramic sherd (4.8 x 3.5 x 0.8 cm). Indicatively, the first two series are presented in greater detail. Included, at the bottom of the figure, is a sub-table listing point composition information as extracted from the Agisoft PhotoScan photogrammetry software (Agisoft LLC) that was used for photo processing and digital modelling.

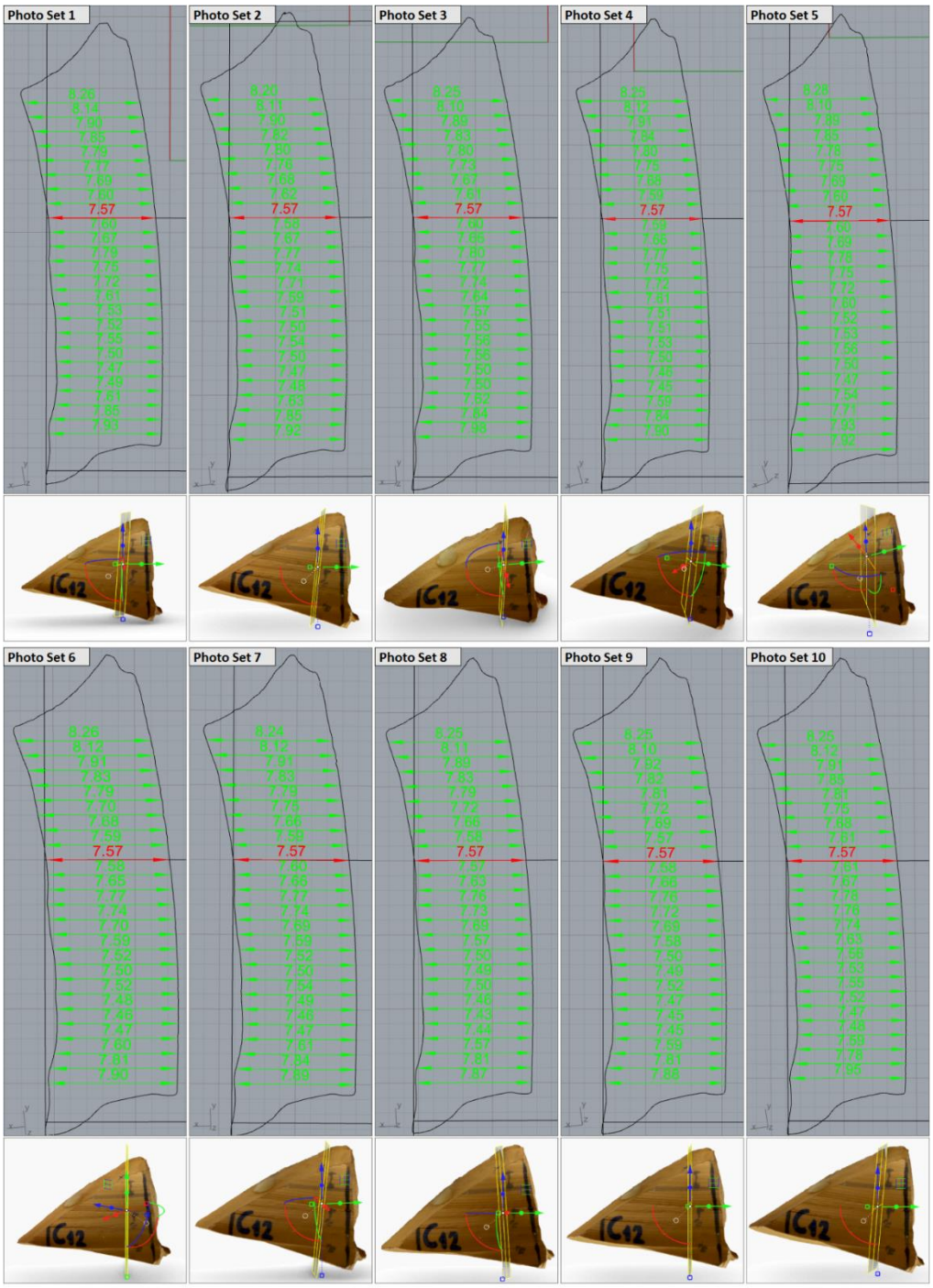

Figure 4. The 10 digital 3D models of the small sherd. The 10 digital cross-sections and the 24 thickness measurements (in hundredths of a millimeter, 0.00 mm). The red measurement of 7.57 mm, in the 9th measurement in a row, represents a known "guide" measurement (the mean value of the 9th measurement in a row, also captured 10 times with the caliper).

Table I. Formulas (2.1) - (2.8), as used in order, for the calculations of the relative quantities in Table III and Table IV (for a population of 10 measurements, N=10).

$\sum_{i=1}^{N} x_i$ (2.1)	$\bar{x} = \frac{1}{N}\sum_{i=1}^{N} x_i$ (2.2)	$\sum_{i=1}^{N} (x_i - \bar{x})$ (2.3)	$\sum_{i=1}^{N} (x_i - \bar{x})^2$ (2.4)
$\delta = \sqrt{\frac{\sum_{i=1}^{N} (x_i - \bar{x})^2}{N-1}}$ (2.5)	$\delta x = \sqrt{\frac{\sum_{i=1}^{N} (x_i - \bar{x})^2}{N(N-1)}}$ (2.6)	$100\frac{\delta x}{\bar{x}}$ % (2.7)	$\bar{x} \pm \delta x$ (2.8)

Sum of Measurements	(2.1)
Mean Value (MV)	(2.2)
Sum of Deviations from MV	(2.3)
Sum of Squared Deviations from MV	(2.4)
Sample Standard Deviation	(2.5)
Uncertainty	(2.6)
Relative Uncertainty	(2.7)
MV Uncertainty	(2.8)

Table II. The 24 thickness measurements (in hundredths of a millimeter, 0.00 mm), as captured 10 times with the caliper. The caliper used in the measurements is calibrated and checked for accuracy using a special ceramic gage block of high precision (grade 1).

	1st	2nd	3rd	4th	5th	6th	7th	8th	9th	10th
1	8,15	8,15	8,16	8,18	8,17	8,16	8,21	8,16	8,17	8,15
2	8,03	8,00	8,06	8,00	8,05	8,05	8,04	8,05	8,02	8,01
3	7,76	7,76	7,77	7,78	7,77	7,77	7,76	7,76	7,76	7,75
4	7,75	7,73	7,73	7,74	7,73	7,73	7,74	7,72	7,72	7,71
5	7,73	7,71	7,73	7,73	7,73	7,73	7,72	7,71	7,71	7,70
6	7,69	7,68	7,70	7,70	7,69	7,70	7,70	7,68	7,66	7,67
7	7,62	7,60	7,59	7,64	7,60	7,62	7,60	7,59	7,59	7,59
8	7,57	7,56	7,58	7,60	7,59	7,59	7,58	7,56	7,55	7,56
9	7,57	7,57	7,57	7,59	7,57	7,57	7,58	7,56	7,56	7,55
10	7,69	7,65	7,64	7,65	7,64	7,64	7,68	7,63	7,63	7,62
11	7,73	7,73	7,73	7,73	7,79	7,72	7,78	7,71	7,78	7,78
12	7,78	7,78	7,78	7,78	7,78	7,78	7,76	7,76	7,74	7,74
13	7,75	7,77	7,79	7,78	7,77	7,77	7,76	7,76	7,75	7,75
14	7,73	7,67	7,65	7,69	7,70	7,74	7,67	7,71	7,65	7,66
15	7,66	7,55	7,56	7,56	7,57	7,59	7,57	7,68	7,54	7,54
16	7,53	7,53	7,55	7,53	7,53	7,51	7,55	7,51	7,50	7,50
17	7,57	7,55	7,58	7,55	7,54	7,52	7,54	7,54	7,53	7,53
18	7,58	7,61	7,61	7,59	7,55	7,56	7,56	7,55	7,55	7,56
19	7,50	7,49	7,50	7,51	7,51	7,51	7,49	7,49	7,51	7,49
20	7,46	7,45	7,49	7,47	7,48	7,49	7,47	7,46	7,45	7,46
21	7,65	7,62	7,61	7,64	7,63	7,65	7,65	7,60	7,58	7,63
22	7,79	7,80	7,80	7,80	7,86	7,78	7,78	7,86	7,88	7,76
23	7,98	7,97	7,98	7,99	7,98	7,97	7,94	7,96	7,97	7,96
24	7,87	7,88	7,89	7,86	7,88	7,90	7,86	7,85	7,84	7,86

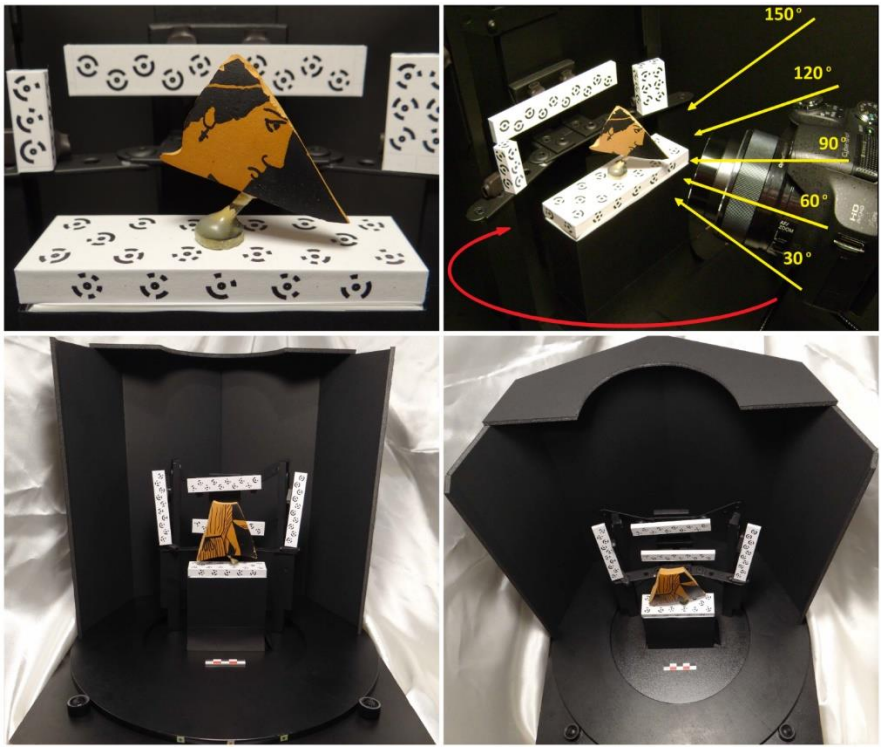

Figure 5. The macrophotography platform.

3. EXPERIMENTAL PROCEDURE

3.1. Photo Shooting Scene

To capture the 10 series of photographs (or photo sets), a laboratory prototype with a basic structure was employed as a photography platform. This structure had dimensions of 50 x 50 x 50 cm and functioned as a manual turntable. It facilitated the rotation of the camera while ensuring the subject and lighting remained stable throughout the photography process. The photography platform is depicted in Fig. 5 and Fig. 6.

The camera used for capturing the photographs was a SONY Cyber-shot DSC-HX100V with a 1/2.3" sensor and a 35mm lens that had a zoom range of 27-810mm and an aperture of F2.8-5.6/4.8-144. The camera featured a macro mode capable of focusing as close as 1cm to the subject. To maintain consistency across shots, a moving background was positioned behind the photographed object, while the camera was moved to ensure that the background remained fixed in all photographs. The camera was placed on a small stable tripod, and the construction materials used for the setup were matte black in color. The photography setup incorporated high-precision metal plates (gage blocks, grade 2) covered with white self-adhesive film to provide a reliable reference for scaling the digital models. The flat surface on which the sherd rested was surrounded by 20-30 small auxiliary targets measuring 0.7 x 0.7 cm each (see Fig. 5, top). These targets served as precision points for the Agisoft PhotoScan photogrammetry software. Lighting was crucial for maintaining accurate and consistent results. A single LED lamp with an intensity of 810 Lumens, emitting warm white light at 3000K, was positioned directly above the photographic object at a height of 25 cm. A thin rice paper was placed in front of the lamp to diffuse the light. It was essential to ensure the stability of both the lighting and the sherd being photographed, as any changes in shadows or lighting conditions could introduce distortions in the digital models. To prevent external light sources, reflections (e.g., from a wristwatch), shadows (e.g., from fingers), and vibrations from affecting the scene, the setup was isolated from such influences. These precautions were taken to minimize potential sources of error in the digital modelling process, as discussed by Guerra (2018) and Percoco et al. (2017).

3.2. The Photo Sets

In *Error Theory* (Rabinovich, 2005), the term *repeatability* refers to the measurement of a quantity under identical observational conditions. This includes using the same instrument, having the same observer, employing the same methodology, maintaining consistent environmental conditions, working with the same subject, and collecting measurements within a relatively short time interval. The term "*method*" encompasses not only the methodology and target positioning but also considers the positioning of the object, lighting conditions, and photographic distance. On

the other hand, the term *reproducibility* is used when measurements are taken under different observational conditions. This involves using different instruments, involving different observers, employing different methodologies, working in different environmental conditions, dealing with different subjects, and collecting measurements over a longer period of time.

Each photo set consists of 116-120 shots captured through a manual cyclical photography process, where each set is taken under different observational conditions. The 120 shots are distributed across 5 shooting levels, with 25 shots allocated to each level. These 5 shooting levels correspond to distinct aiming angles of the camera in relation to the object, namely 30°, 60°, 90°, 120°, and 150° (see Fig. 5, top right). Prior to capturing each photo set, the sherd was repositioned, meaning it was placed in a different position within the set. This ensured that each series of photographs differed significantly from the others. The targets used for the photogrammetry software were also slightly repositioned with each new series of photographs. Similarly, the lighting setup underwent slight positional changes for each new series of photographs. By introducing variations in these parameters, such as the sherd's position, the position of the targets, and the lighting, the intention was to minimize the influence of *repeatability* on the overall process.

The 10 series of photography were captured at sporadic intervals over the course of three consecutive days during the approximate evening hours. Throughout these sessions, the environmental conditions, including temperature, softly fluctuated, and there were also insignificant variations in atmospheric pressure and relative humidity (see Fig. 3, bottom right, sub-table).

It is important to note that significant variations in temperature, pressure, and humidity can have an impact on the photogrammetry setup, given its reliance on precise metal gage blocks. These conditions can also potentially affect the metal arm supporting the lighting, the rotating plate, and the surrounding metal structure that supports and encloses the sherd. If there were significant deviations in these conditions, it would introduce *random error factors* into the measurements, such as temperature and atmospheric pressure. This, in turn, could unnecessarily increase the overall error of the measurements. Hence, efforts were made to maintain a consistent environment to minimize these potential sources of error.

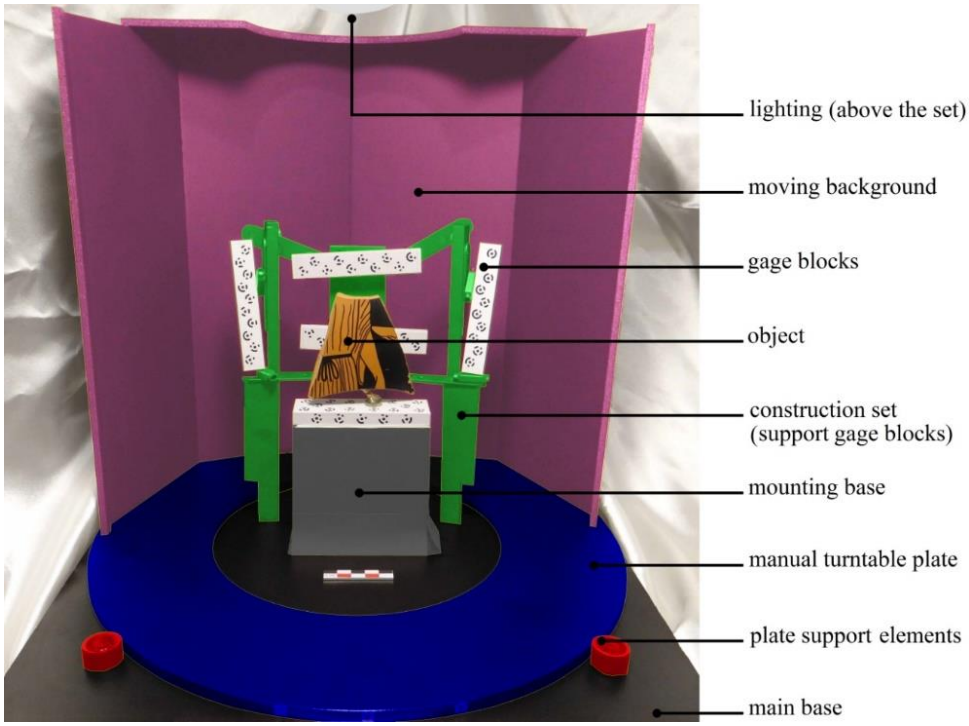

Figure 6. The photographic setup (deliberately coloured per section of interest).

Table III. The 24 uncertainties and errors of the thickness measurements, from 10 digital 3D models. The calculations from formulas (2.1) - (2.8), on Table I.

	(2.1)	(2.2)	(2.3)	(2.4)	(2.5)	(2.6)	(2.7)	(2.8)
1	82,49	8,249	0	$3,69x10^{-3}$ mm²	0,02024846	0,00640312mm	0,078%	**8,25±0,01mm**
2	81,14	8,114	0	$1,44x10^{-3}$ mm²	0,01264911	0,00400000mm	0,049%	**8,11±0,00mm**
3	79,03	7,903	0	$1,01x10^{-3}$ mm²	0,01059350	0,00334996mm	0,042%	**7,90±0,00mm**
4	78,35	7,835	0	$1,25x10^{-3}$ mm²	0,01178511	0,00372678mm	0,048%	**7,84±0,00mm**
5	77,96	7,796	0	$0,84x10^{-3}$ mm²	0,00966092	0,00305505mm	0,039%	**7,80±0,00mm**
6	77,40	7,740	0	$4,20x10^{-3}$ mm²	0,02160247	0,00683130mm	0,088%	**7,74±0,01mm**
7	76,78	7,678	0	$1,16x10^{-3}$ mm²	0,01135292	0,00359011mm	0,047%	**7,68±0,00mm**
8	75,96	7,596	0	$2,04x10^{-3}$ mm²	0,01505545	0,00476095mm	0,063%	**7,60±0,01mm**
9*	**75,70**	**7,570**	0	$0,00x10^{-3}$ mm²	0,00000000	0,00000000mm	0,000%	**7,57±0,00mm**
10	75,91	7,591	0	$1,49x10^{-3}$ mm²	0,01286684	0,00406885mm	0,054%	**7,59±0,00mm**
11	76,62	7,662	0	$2,16x10^{-3}$ mm²	0,01549193	0,00489898mm	0,064%	**7,66±0,01mm**
12	77,75	7,775	0	$1,45x10^{-3}$ mm²	0,01269296	0,00401386mm	0,052%	**7,78±0,00mm**
13	77,45	7,745	0	$1,85x10^{-3}$ mm²	0,01433721	0,00453382mm	0,059%	**7,75±0,01mm**
14	77,12	7,712	0	$3,36x10^{-3}$ mm²	0,01932184	0,00611010mm	0,079%	**7,71±0,01mm**
15	76,01	7,601	0	$4,29x10^{-3}$ mm²	0,02183270	0,00690411mm	0,091%	**7,60±0,01mm**
16	75,24	7,524	0	$5,04x10^{-3}$ mm²	0,02366432	0,00748331mm	0,099%	**7,52±0,01mm**
17	75,12	7,512	0	$3,56x10^{-3}$ mm²	0,01988858	0,00628932mm	0,084%	**7,51±0,01mm**
18	75,37	7,537	0	$3,41x10^{-3}$ mm²	0,01946507	0,00615540mm	0,082%	**7,54±0,01mm**
19	74,98	7,498	0	$6,96x10^{-3}$ mm²	0,02780887	0,00879394mm	0,117%	**7,50±0,01mm**
20	74,64	7,464	0	$2,84x10^{-3}$ mm²	0,01776388	0,00561743mm	0,075%	**7,46±0,01mm**
21	74,77	7,477	0	$7,61x10^{-3}$ mm²	0,02907844	0,00919541mm	0,123%	**7,48±0,01mm**
22	76,12	7,612	0	$13,36x10^{-3}$ mm²	0,03852849	0,01218378mm	0,160%	**7,61±0,01mm**
23	78,36	7,836	0	$14,44x10^{-3}$ mm²	0,04005552	0,01266667mm	0,162%	**7,84±0,01mm**
24	79,14	7,914	0	$10,04x10^{-3}$ mm²	0,03339993	0,01056199mm	0,133%	**7,91±0,01mm**

Table IV. The 24 uncertainties and errors of thickness measurements, from 10 consecutive caliper measurements. The calculations from formulas (2.1) - (2.8), on Table I.

	(2.1)	(2.2)	(2.3)	(2.4)	(2.5)	(2.6)	(2.7)	(2.8)
1	81,66	8,166	0	$3,04x10^{-3}$ mm²	0,01837873	0,00581187mm	0,071%	**8,17±0,01mm**
2	80,31	8,031	0	$4,49x10^{-3}$ mm²	0,02233582	0,00706321mm	0,088%	**8,03±0,01mm**
3	77,64	7,764	0	$0,64x10^{-3}$ mm²	0,00843274	0,00266667mm	0,034%	**7,76±0,00mm**
4	77,30	7,730	0	$1,20x10^{-3}$ mm²	0,01154701	0,00365148mm	0,047%	**7,73±0,00mm**
5	77,20	7,720	0	$1,20x10^{-3}$ mm²	0,01154701	0,00365148mm	0,047%	**7,72±0,00mm**
6	76,87	7,687	0	$1,81x10^{-3}$ mm²	0,01418136	0,00448454mm	0,058%	**7,69±0,00mm**
7	76,04	7,604	0	$2,64x10^{-3}$ mm²	0,01712698	0,00541603mm	0,071%	**7,60±0,01mm**
8	75,74	7,574	0	$2,44x10^{-3}$ mm²	0,01646545	0,00520683mm	0,069%	**7,57±0,01mm**
9*	75,69	7,569	0	$1,09x10^{-3}$ mm²	0,01100505	0,00348010mm	0,046%	**7,57±0,00mm**
10	76,47	7,647	0	$4,41x10^{-3}$ mm²	0,02213594	0,00700000mm	0,092%	**7,65±0,01mm**
11	77,48	7,748	0	$8,36x10^{-3}$ mm²	0,03047768	0,00963789mm	0,124%	**7,75±0,01mm**
12	77,68	7,768	0	$2,56x10^{-3}$ mm²	0,01686548	0,00533333mm	0,069%	**7,77±0,01mm**
13	77,65	7,765	0	$1,65x10^{-3}$ mm²	0,01354006	0,00428174mm	0,055%	**7,77±0,00mm**
14	76,87	7,687	0	$9,41x10^{-3}$ mm²	0,03233505	0,01022524mm	0,133%	**7,69±0,01mm**
15	75,82	7,582	0	$21,56x10^{-3}$ mm²	0,04894441	0,01547758mm	0,204%	**7,58±0,02mm**
16	75,24	7,524	0	$3,04x10^{-3}$ mm²	0,01837873	0,00581187mm	0,077%	**7,52±0,01mm**
17	75,45	7,545	0	$3,05x10^{-3}$ mm²	0,01840894	0,00582142mm	0,077%	**7,55±0,01mm**
18	75,72	7,572	0	$5,16x10^{-3}$ mm²	0,02394438	0,00757188mm	0,100%	**7,57±0,01mm**
19	75,00	7,500	0	$0,80x10^{-3}$ mm²	0,00942809	0,00298142mm	0,040%	**7,50±0,00mm**
20	74,68	7,468	0	$1,96x10^{-3}$ mm²	0,01475730	0,00466667mm	0,062%	**7,47±0,01mm**
21	76,26	7,626	0	$5,04x10^{-3}$ mm²	0,02366432	0,00748331mm	0,098%	**7,63±0,01mm**
22	78,11	7,811	0	$14,89x10^{-3}$ mm²	0,04067486	0,01286252mm	0,165%	**7,81±0,01mm**
23	79,70	7,970	0	$1,80x10^{-3}$ mm²	0,01414214	0,00447214mm	0,056%	**7,97±0,00mm**
24	78,69	7,869	0	$3,09x10^{-3}$ mm²	0,01852926	0,00585947mm	0,074%	**7,87±0,01mm**

3.3. Calculations and Result Comparisons

By comparing the uncertainties presented in Tables III and IV, which consist of 24 values each, it becomes possible to assess the potential error associated with the photogrammetry process. This comparison allows for drawing conclusions regarding the overall similarity of the measurements. In order to facilitate visualization and evaluation of the final conclusions, column (2.8) from both Tables III and IV is displayed with rounding to two decimal digits. Additionally, on Tables III and IV the values in last column are highlighted using three different colors to aid in their distinction and interpretation (green, yellow and red). The reader may also notice that the 9th measurement is marked with an asterisk. This is due to the fact that this measurement (9th), is intentionally selected to represent a known "*guide*" measurement (i.e. reference measurement). It has been obtained by taking the mean value of the 9th measurement, which was measured 10 times with the caliper. The value of this measurement is recorded as 7.57 mm. Upon analyzing the calculations for the 8th, 9th*, 12th, 13th, 14th, 15th, 16th, 18th, 19th, and 20th consecutive readings, it can be observed that the average values exhibit marginal deviations between the digital and real-world data. These readings are highlighted in green color to indicate convergence, signifying a close match between the average values. Notably, the 9th*, 16th, and 19th series of measurements demonstrate an absolute match in the average values. For the remaining series highlighted in green (8th, 12th, 13th, 14th, 15th, 18th, and 20th), the average values deviate slightly, ranging from 0.01 mm to 0.03 mm. These deviations, although present, are still within a small margin. On the other hand, the average values highlighted in yellow, calculated from the 1st, 2nd, 5th, 6th, 7th, 10th, 11th, 17th, and 24th consecutive readings, exhibit larger deviations between the digital and real data. These deviations range from 0.04 mm to 0.09 mm. The red highlight is applied to the calculations corresponding to the 3rd, 4th, 21st, 22nd, and 23rd consecutive measurements. These measurements exhibit average value deviations ranging from 0.11 mm to 0.15 mm. Among these series, the 22nd measurement stands out as it deviates by 0.20 mm. Overall, these findings provide insight into the accuracy and consistency of the photogrammetry measurements compared to the known "*guide*" measurement obtained with the caliper. By examining all these deviations, it is possible to gain insights into the level of accuracy and consistency achieved by the photogrammetry process in relation to the real-world data.

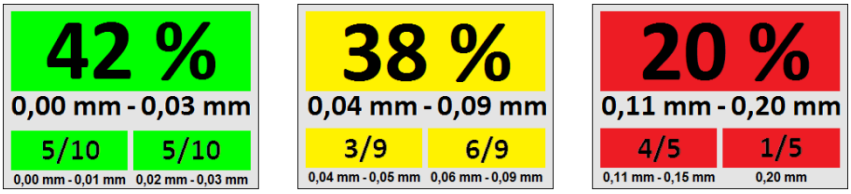

Figure 7. Final result comparison, between Table III and Table IV.

Based on the observations made, Fig. 7 depicts that:

- Approximately 42% of all 24 thickness measurements and uncertainty calculations show a deviation of the average value measurements between the digital model and the real world that is almost zero. This deviation in half of the cases of 42%, ranges from 0.00 mm to 0.01 mm. In the remaining cases within the 42%, the deviation of the average value measurements does not exceed 0.03 mm.
- For about 38% of the 24 thickness measurements, the deviation of the average value measurements does not exceed 0.09 mm.
- In the remaining 20% of the total 24 measurements, the deviation of the average value measurements between the digital model and the real world does not exceed 0.20 mm.

Fig. 8 is a graphical representation that combines the final calculations on Table III and Table IV, using formula (2.8) from Table I. The graph shows the dispersion of the measurements at each of the 24 measurement points and the deviations between the caliper and the digital models. In the graph, the measurements obtained with the caliper are represented in red, the measurements from the digital models are represented in blue, and the points where the calculations coincide are represented in magenta. In the center of the graph, there is a vertical green line that represents an ideal situation where the calculations from both the caliper and the 3D models coincide exactly at the same values for all 24 measurement points. This represents a situation of absolute accuracy and reliability. On the left side of the graph, the data is presented with rounded values in hundredths of a millimeter (0.00 mm) as they were during the calculation process. On the right side of the graph, the same data is presented in thousandths of a millimeter (0.000 mm), as they were initially calculated. In the measurement process, it is important to consider the potential sources of error. One such factor is the error associated with the caliper, which has a precision of ±0.02 mm. This means that the measurements obtained using the caliper have an uncertainty of ±0.02 mm. Considering this uncertainty, it is reasonable to assign an overall uncertainty

of ±0.02 mm to the 24 thickness measurements presented in both Tables III and IV. This value takes precedence over any smaller uncertainties observed in the experiments. By accounting for the caliper's error and including the ±0.02 mm uncertainty, the analysis becomes more comprehensive and ensures that the measurements are evaluated within an appropriate range.

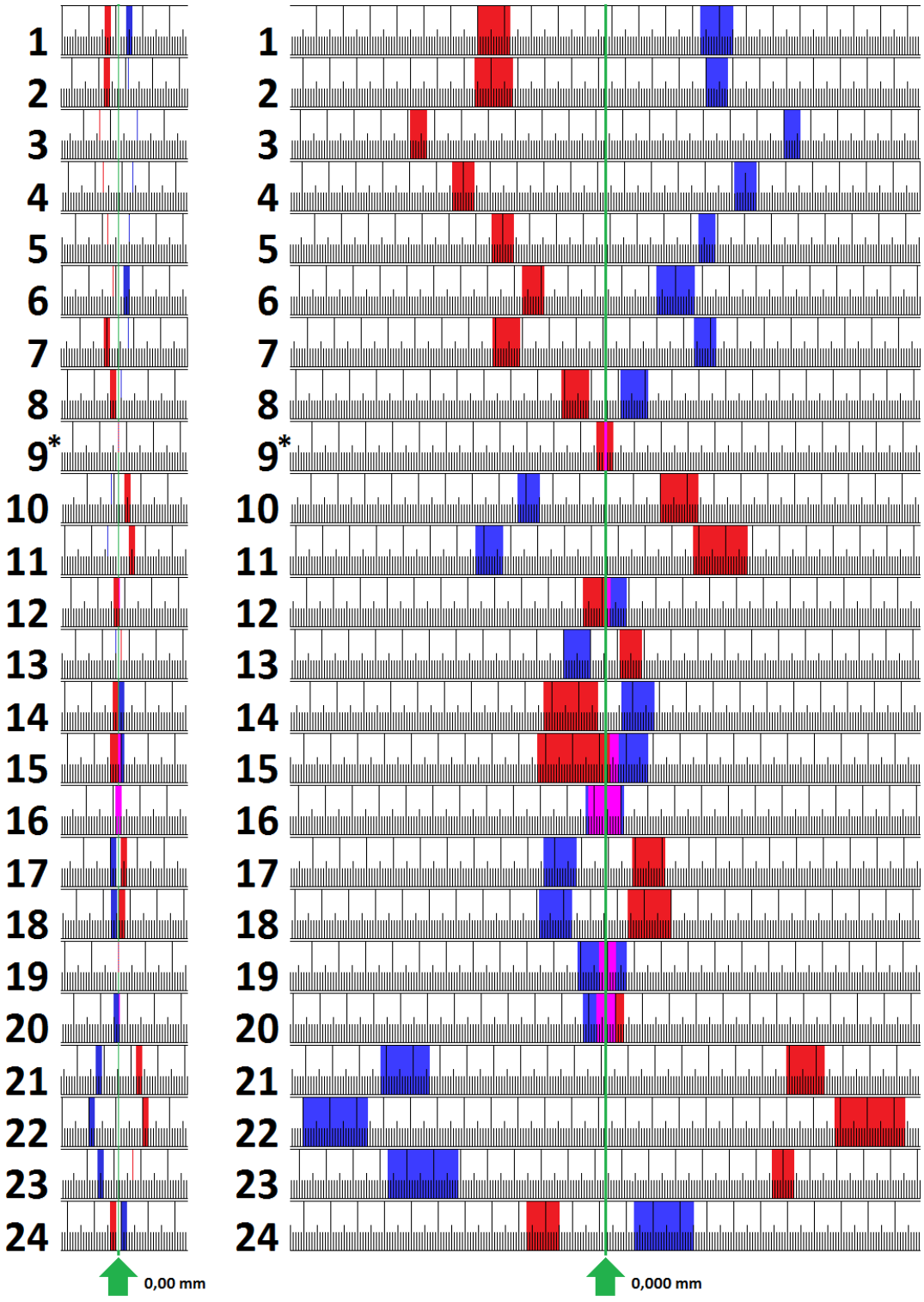

Figure 8. Comparing the two sets of final calculations, from formula (2.8), in a holistic graphical representation. In red, the caliper, in blue the macrophotogrammetry and in magenta, points where the calculations coincide.

4. CONCLUSIONS

This paper presents the results of a comprehensive experiment conducted to assess the reliability of photogrammetry in modelling small objects. The findings indicate that photogrammetry yields highly accurate results that closely match reality. What's more, it doesn't necessitate expensive photographic equipment or specialized software, and no specialized knowledge is required for illuminating the objects during photography.

The quality of digital models produced using photogrammetry for small objects is on par with, and possibly even superior to, that of optical scanners such as laser scanners and 3D scanners. These scanning technologies typically come with substantial costs, both for the equipment itself and for maintenance and training (Ravanelli et al., 2017). In contrast, photogrammetry offers a cost-effective and accessible alternative.

Based on these findings, it is clear that in the coming years, the use of photogrammetry and macrophotography for digital modelling of small-scale objects will likely experience significant advancements. This technique holds great potential for various fields of science, particularly in information technology and archaeological excavations (Psarros et al., 2022).

AUTHORS CONTRIBUTION: Conceptualization, M.I.S. and C.N.A.; methodology, M.I.S. and C.N.A.; software, M.I.S.; validation, M.I.S.; formal analysis, M.I.S.; investigation, M.I.S.; resources, M.I.S. and C.N.A.; data curation, M.I.S.; writing—original draft preparation, M.I.S.; writing—review and editing, C.N.A.; visualization, M.I.S..; supervision, C.N.A.; project administration, C.N.A.; funding acquisition, M.I.S and C.N.A. All authors have read and agreed to the published version of the manuscript.

ACKNOWLEDGEMENT

The authors thank the anonymous reviewers for their constructive comments. The research of this paper was financially supported by the General Secretariat for Research and Technology (GSRT), through the research project "Advanced system for multimodal Recording, Documentation and Promotion of Archaeological Work" (Τ6ΥΒΠ-00439, MIS 5056317), Framework "Special Actions in aquaculture, industrial materials and open innovation in culture", Operational Program "Competitiveness Entrepreneurship and Innovation", 2014-2021 "Development of Entrepreneurship with Sectoral Priorities", co-financed by the European Regional Development Fund (ERDF) and from National Resources. The funders had no role in study design, data collection and analysis, decision to publish, or preparation of the manuscript.

REFERENCES

Bevington, P., Robinson, K. (2003) *Data Reduction and Error Analysis for the Physical Sciences*. The McGraw-Hill Companies Inc., 3rd edn., ISBN 0-07247227-8.

BIPM, IEC, IFCC, ISO, IUPAC, IUPAP, and OIML. (1995) *Guide to the expression of uncertainty in measurement*. 2nd edn., ISBN 92-67-10188-9.

BIPM, IEC, IFCC, ILAC, ISO, IUPAC, IUPAP and OIML. (2020) *Guide to the expression of uncertainty in measurement — Part 6: Developing and using measurement models.* JCGM GUM-6:2020.

Cramer, M. (2013) The UAV @ LGL BW project-A NMCA case study. In: *Proceedings of the 54th Photogrammetric Week*, pp.165-179, Stuttgart, Germany.

Gajski, D., Solter, A., Gasparovic, M. (2016) Applications of Macro Photogrammetry in Archaeology. *The International Archives of the Photogrammetry, Remote Sensing and Spatial Information Sciences*, Vol. XLI-B5, XXIII ISPRS Congress, DOI:10.5194/isprsarchives-XLI-B5-263-2016, Prague, Czech Republic.

Gontard, C., Batista, M., Salguero, J., Calvino, J. (2018) Three-dimensional chemical mapping using non-destructive SEM and photogrammetry. *Scientific Reports*, Vol. 8, Article 11000.

Guerra, M.G. (2018) Analysis of a 3D optical scanner based on photogrammetry suitable for industrial applications in close and micro-range. Politecnico di Bari, Department of Mechanics, Mathematics and Management Mechanical and Management Engineering, Ph.D. Thesis SSD ING-IND/16.

Jing, X., Zhang, C., Sun, Z., Zhao, G., Wang, Y. (2015) The Technologies of Close-range Photogrammetry and Application in Manufacture. *Proceedings of the 3rd International Conference on Mechatronics, Robotics and Automation* - ICMRA 2015.

Kraus, K. (2007) *Photogrammetry: Geometry from images and Laser Scans*. Walter de Gruyter.

Luhmann, T. (2010) Close range photogrammetry for industrial applications. *ISPRS Journal of Photogrammetry and Remote Sensing,* 65(6), 558-569.

Mallison, H., Wings, O. (2014) Photogrammetry in Paleontology - A Practical Guide. *Journal of Paleontological Techniques,* 12, 1-31.

Marziali, S., Dionisio, G. (2017) Photogrammetry and Macro Photography. The Experience of the MUSINT II Project in the 3D Digitization of Small Archaeological Artifacts. SDH *Open Access Journal Studies in Digital Heritage,* 1(2), DOI:10.14434/sdh.v1i2.23250.

Mendikute, A., Yague-Fabra, J., Zatarain, M., Bertelsen, A., Leizea, I. (2017) Self-Calibrated In-Process Photogrammetry for Large Raw Part Measurement and Alignment before Machining. *Sensors*, 17(9):2066, DOI:10.3390/s17092066.

Mikerov, M., Shrestha, R., Dommelen, R., Mittleman, D., Koch, M. (2020) Analysis of ancient ceramics using terahertz imaging and photogrammetry. *Optics Express* Vol. 28, Issue 15, pp. 22255-22263, https://doi.org/10.1364/OE.399336.

Murtiyoso, A., Grussenmeyer, P., Borlin, N. (2017) Reprocessing Close Range Terrestrial and UAV Photogrammetric Projects with the DBAT Toolbox for Independent Verification and Quality Control. The International Archives of the Photogrammetry, Remote Sensing and Spatial Information Sciences, Vol. XLII-2/W8, *2017 5th International Workshop LowCost 3D - Sensors, Algorithms, Applications*, Hamburg, Germany.

Peggs, N., Maropoulos, G., Hughes, B., Forbes, B., Robson, S., Ziebart, M., et al. (2009) Recent developments in large-scale dimensional metrology. *Proceedings of the Institution of Mechanical Engineers Part B Journal of Engineering Manufacture,* 223(6), 571-595.

Percoco, G., Guerra, M.G., Salmeron, A.J., Galantucci, L.M. (2017) Experimental investigation on camera calibration for 3D photogrammetric scanning of micro-features for micrometric resolution. *The International Journal of Advanced Manufacturing Technology,* 91(9-12), 2935-2947.

Plum, F., Labonte, D. (2021) scAnt-an open-source platform for the creation of 3D models of arthropods (and other small objects). P*eerJ* 9:e11155, DOI:10.7717/peerj.11155.

Psarros, D., Stamatopoulos M.I., Anagnostopoulos C.N. (2022) Information technology and archaeological excavations: a brief overview, *Scientific Culture* Vol. 8, no. 2, pp. 147-167, DOI: 10.5281/zenodo.6323149.

Puhar, E., Eric, M., Kavkler, K., Cramer, A., Celec, K., Korat, L., Jaklic, A., Solina, F. (2018) Comparison and deformation analysis of five 3D models of the Paleolithic wooden point from the Ljubljanica River. 2018 IEEE *International Conference on Metrology for Archaeology and Cultural Heritage,* (MetroArchaeo 2018), Cassino, Italy.

Quattrini, R., Nespeca, R., Ruggeri, L. (2017) Digital photogrammetry for archaeological artefacts acquisition. IMEKO International Conference on Metrology for Archaeology and Cultural Heritage, Lecce, Italy.

Rabinovich, S. (2005) *Measurement Errors and Uncertainties Theory and Practice*. Springer, 3rd edn, ISBN-13: 978-0387-25368-9, ISBN-10: 0-387-25358-0.

Ravanelli, R., Di Rita, M., Nascetti, A., Crespi, M., Nigro, L., Montanari D., Spagnoli, F. (2017) Penguin 3.0 – Capturing Small Finds in 3D. *Mediterranean Archaeology and Archaeometry*, Vol. 17, No 2, pp. 49-56, DOI:10.5281/zenodo.581720.

Ray, F. (2002) *Applied Photography Optics*. Focal Press, 3rd edn, ISBN 13: 978-0240515403, ISBN 10: 0240515404.

Remondino, F., Del Pizzo, S., Kersten, T., Troisi, S. (2012) Low-cost and open-source solutions for automated image orientation - A critical overview. *Proccedings EuroMed 2012 Conference*, LNCS 7616, pp. 40-54, DOI:10.1007/978-3-642-34234-9_5.

Samaan, M., Heno, R., Pierrot-Deseilligny, M. (2013) Close-Range Photogrammetric Tools For Small 3D Archaeological Objects. International Archives of the Photogrammetry, Remote Sensing and Spatial Information Sciences, Vol. XL-5/W2, XXIV International CIPA Symposium, Strasbourg, France.

Santella, M., Milner, A. (2017) Coupling Focus Stacking with Photogrammetry to Illustrate Small Fossil Teeth. *Journal of Paleontological Techniques,* Number 18, ISSN: 1646-5806.

Stamatopoulos, M., Anagnostopoulos, C. (2017) A totally new digital 3D approach for reassembling fractured archaeological potteries using thickness measurements. *Acta IMEKO* 6(3), 18–28.

Stamatopoulos, M., Anagnostopoulos, C. (2018) Simulation of an Archaeological Disaster: Reassembling a Fragmented Amphora using the Thickness Profile Method. *Proceedings of 7th International Euro-Mediterranean Conference on Digital Heritage - EuroMed 2018*, pp. 162-173, Nicosia, Cyprus.

Stamatopoulos, C., Fraser, S. (2011) Calibration of Long Focal Length Cameras in Close Range Photogrammetry. *The Photogrammetric Record*, 26(135), 339-360.

Stamatopoulos, C., Fraser, S. (2014) Automated Target-free Network Orientation and Camera Calibration. ISPRS Annals of the Photogrammetry, Remote Sensing and Spatial Information Sciences, Vol. II-5, 2014 ISPRS Technical Commission V Symposium, DOI:10.1111/j.1477-9730.2011.00648.x, Riva del Garda, Italy.

Vaezi, M. Seitz, H. Yang, S. (2013) A review on 3D micro-additive manufacturing technologies. *The International Journal of Advanced Manufacturing Technology,* 67(5-8), 1721-1754, DOI:10.1007/s00170-012-4605-2.

Verma, A., Bourke, M. (2019) A method based on structure-from-motion photogrammetry to generate sub-millimetre-resolution digital elevation models for investigating rock breakdown features. *Earth Surface Dynamics*, 7, pp. 45-66.

Xu, A., Dudek, G. (2011) Fourier Tag: A Smoothly Degradable Fiducial Marker System with Configurable Payload Capacity. *2011 Canadian Conference on Computer and Robot Vision*, IEEE, DOI:10.1109/CRV.2011.13.

Yanagi, H., Chikatsu, H. (2010) 3D Modelling of small objects using macro lens in digital very close range photogrammetry. *International Archives of Photogrammetry, Remote Sensing and Spatial Information Sciences*, Vol. XXXVIII, Part 5 Commission V Symposium, Newcastle upon Tyne, U.K.